Journal of Structural Geology 33 (2011) 1627–1638

Contents lists available at SciVerse ScienceDirect

Journal of Structural Geology

journal homepage: www.elsevier.com/locate/jsg

# Geometry, microstructures, and magnetic fabrics of kink bands in the Darrington Phyllite, northwestern Washington, USA: Processes within fixed-hinge kinking

Rachel E. Dunham[a,*], Juliet G. Crider[b], Russell F. Burmester[a], Elizabeth R. Schermer[a], Bernard A. Housen[a]

[a] Department of Geology, Western Washington University, 516 High St. MS 9080, Bellingham, WA 98225, USA
[b] Department of Earth and Space Sciences, University of Washington, Box 351310, Seattle, WA 98195, USA

ARTICLE INFO

*Article history:*
Received 19 January 2011
Received in revised form
18 August 2011
Accepted 30 August 2011
Available online 16 September 2011

*Keywords:*
Kink band
Phyllite
Deformation
Magnetic anisotropy
Thin section
Microfabric

ABSTRACT

Field, thin section, and magnetic fabric analyses of monoclinal, contractional kink bands in the Darrington Phyllite of northwestern Washington, USA, provide evidence of kinematic evolution and microstructural processes during kinking. Relationships among internal, external, and rotation angles of kink bands suggest that rotation was a primary mechanism of kinking, and a significant number of kink bands deviate from the "ideal" kink band geometry (equal internal and external kink angles). Dilation spaces (voids) filled with unrecrystallized quartz and/or calcite inside kink bands and along the boundaries are commonly observed in kink bands with unequal kink angles. Evidence for localized interlayer slip inside kink bands includes mica grains protruding into the hinge voids and stair-step geometry of the voids. Interlayer slip allowed for rotation of the internal foliation during kinking. Pressure solution is not ubiquitous inside kink bands from the study area; however, significant pressure solution is associated with "locked" kink bands (equal kink angles). A new approach using the anisotropy of magnetic susceptibility (AMS) shows that the magnetic fabric and susceptibility inside the kink bands differ more from the outside fabric than can be explained by simple rotation of the outside fabric into the kink attitudes. Combined, our observations suggest that fixed-hinge kinking operated at this location, and that veining, interlayer slip, and pressure solution were the dominant deformation mechanisms.



## 1. Introduction

Kink bands are common structures in contractional deformation zones, but mechanism(s) of kinking at both the macro- and micro-scales are poorly understood. Despite a rich literature in field observations and deformation experiments, few studies report analyses of the microfabrics within kink bands that could illuminate the processes of kink band growth. Thin section and magnetic fabric analyses have been performed on kink bands (e.g. Paterson and Weiss, 1966; Verbeek, 1978; Stewart and Alvarez, 1991; Kirker and McClelland, 1997); here we advance this work by connecting observed microfabrics associated with kink bands to specific kinking mechanism(s).

Kink bands are small monoclinal folds with sharp parallel hinges (Fig. 1) that occur in fine-grained, anisotropic rocks. Both contractional and extensional kink bands are possible (Dewey, 1965); this paper focuses only on the characteristics of contractional kink bands. A single kink band consists of two long (undeformed) limbs bracketing a shorter "kinked" (deformed) limb, and the traces of the axial planes of the hinges mark the boundaries of the kink band. Previous workers have defined a number of angles in kink bands (e.g. Verbeek, 1978; Fig. 1): the external (acute) angle ($\alpha$) between the undeformed foliation and the kink band boundary; the internal angle ($\beta$) between the kinked foliation and the boundary; and the rotation angle ($\kappa$) through which the kinked foliation has been rotated, where $\kappa = 180^\circ - \alpha - \beta$ (Weiss, 1980).

Field studies of kink bands (e.g. Anderson, 1964; Clifford, 1968; Fyson, 1968; Hobson, 1973; Verbeek, 1978; Kirschner and Teixell, 1996) have focused mainly on outcrop-scale features and geometries, usually qualitatively and in the context of a regional deformation framework. Analog and rock experiments (e.g. Paterson and Weiss, 1966; Anderson, 1974; Stewart and Alvarez, 1991) provided some observations of microstructures and fabric in thin section, but detailed descriptions of natural kink bands in thin section are uncommon in the literature. Observations on the geometry of kink bands have been used to propose and evaluate models for kink band development (e.g. Dewey, 1965; Verbeek, 1978; Weiss, 1980; Stewart and Alvarez, 1991), generally focusing on the angular relationships between the foliation and the kink band boundaries and only marginally on the grain-scale characteristics of the rocks.

* Corresponding author. Tel.: +1 650 207 0908.
*E-mail address:* rachel.dunham@gmail.com (R.E. Dunham).

0191-8141/$ – see front matter © 2011 Elsevier Ltd. All rights reserved.
doi:10.1016/j.jsg.2011.08.010

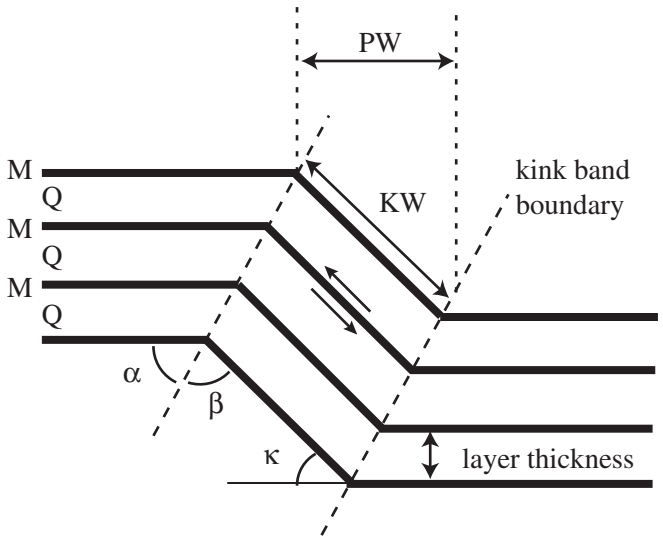


**Fig. 1.** Schematic kink band showing parameters measured in thin section and in the field. The angles α and β are the external and internal angles, respectively, between the foliation and the kink band boundaries; κ is the angle through which the kinked foliation has rotated. The kinked width (KW) and plan width (PW) are measured relative to the kink band boundaries. Foliation spacing is measured as the average thickness of quartz layers (Q) bounded by thin mica horizons (M). Arrows inside kink band show expected slip direction for a dextral kink band.

Microstructures and magnetic fabrics related to kink bands can yield information on deformation mechanisms and strain within the kink bands (e.g. Stewart and Alvarez, 1991; Kirker and McClelland, 1997), which can be related to kink band geometry and models of kink band development.

The mechanics by which kink bands develop are unresolved; previous workers have generally adhered to one of two major kinematic models. The mobile-hinge model of kinking has been championed by many (e.g. Paterson and Weiss, 1966; Weiss, 1980; Stewart and Alvarez, 1991). In this model, kink bands accommodate shortening by incorporating new material as the hinges migrate outward into the external (undeformed) medium and material is folded and then unfolded as the kink band widens (Weiss, 1980). Evidence for hinge migration has been seen in thin section (Paterson and Weiss, 1966) and in deformation experiments (Paterson and Weiss, 1966; Gay and Weiss, 1974; Stewart and Alvarez, 1991). The geometric constraints of the mobile-hinge model require zero dilation inside the kink band and equal kink angles α and β (see Fig. 1). The fixed-hinge model of kinking has been invoked in several field-based studies (e.g. Dewey, 1965; Hobson, 1973; Verbeek, 1978). Kink bands in this model develop via rigid rotation of the internal foliation between two fixed hinges. This requires dilation between the internal foliation planes and along the kink band boundaries at low rotation angles when $\beta > \alpha$; deformation ceases when the kink band "locks" at $\beta = \alpha$ (Verbeek, 1978; Stewart and Alvarez, 1991). For both models, kink bands with equal angles α and β are taken as the "ideal" (mobile-hinge) or "locked" (fixed-hinge) case. In fixed-hinge kinking, kink bands with low rotation angles and $\beta > \alpha$ are in the early stages of formation. The case $\beta < \alpha$ is not permitted by either model, but may occur due to syn- or post-kinking rotation or slip of the outside foliation (Gay and Weiss, 1974; Rousell, 1980; Stewart and Alvarez, 1991). Both the mobile- and fixed-hinge kinking models require interlayer slip inside the kink band (Paterson and Weiss, 1966; Weiss, 1980; Stewart and Alvarez, 1991), sinistral slip inside dextral kink bands (Fig. 1) and vice versa (e.g. Verbeek, 1978; Rousell, 1980). Some workers have argued that both mechanisms operate under different conditions, depending on the amount of strain accommodated (Stewart and Alvarez, 1991) or the confining pressure of the rocks at the time of kinking (Anderson, 1974). It is also possible to imagine hybrid kinematics that involve both rotation of the kinked limb and migration of its boundaries (e.g. Twiss and Moores, 1992). The role of other mechanisms (e.g. pressure solution) is poorly addressed, though Stewart and Alvarez (1991) suggest that pressure solution could be invoked as a hinge-migration mechanism.

We use field, thin section, and magnetic fabric analyses to characterize the macro- and micro-scale features of kink bands in the Darrington Phyllite of northwestern Washington in order to understand what processes operate on the grain scale within kink bands and how the rock characteristics affect the formation of kink bands. Field and thin section observations provide a detailed record of the variations in kink band geometry and related features. We also present a new method that examines magnetic fabrics from outside and inside kink bands to quantify changes due to kinking. These observations are used to assess whether interlayer slip and/or pressure solution occurred during kinking. The characteristics of the kink bands are also used to evaluate the applicability of the mobile- and/or fixed-hinge kinking models to the kink bands in the Darrington Phyllite.

## 2. Study area

A dense network of monoclinal kink bands records late deformation of a well-developed foliation in the Darrington Phyllite on Samish Island in northwestern Washington (Fig. 2). The Darrington Phyllite is part of the Shuksan Metamorphic Suite (Misch, 1966; Brown, 1986; Gallagher et al., 1988), which comprises ocean floor sedimentary and igneous rocks that have undergone subduction-related metamorphism and several subsequent deformation events (Haugerud, 1980; Haugerud et al., 1981; Brown, 1986). On Samish Island, the Darrington Phyllite is a micaceous quartzose phyllite that underwent blueschist-facies metamorphism at ~154 Ma (Lamb, 2000). Metamorphism and recrystallization are

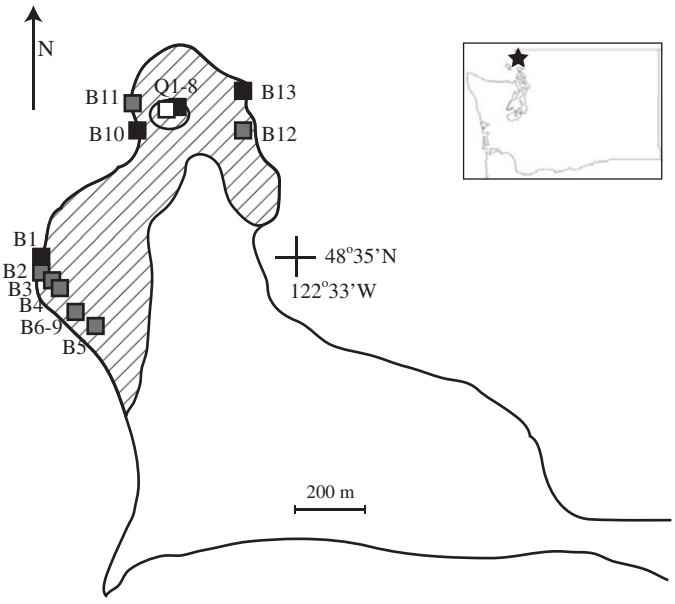


**Fig. 2.** Schematic geologic map of Samish Island; location within Washington state is shown by the black star on inset. Jurassic bedrock (Darrington Phyllite; hachured area) is exposed only on the northern point of the island as beach outcrops and in a quarry (circle); the remainder of the island consists mainly of Quaternary glacial deposits. Locations where detailed field measurements were made are marked with gray squares, those sampled for thin section by black squares, and those for AMS analyses by the white square. Geology from Jones (1999).

sufficiently intense that the original sedimentary layering of the rock is obscured, although there is a broad trend of increasing grain size and increased quartz from NE to SW in the exposed rocks (Lamb, 2000). The structural history of Samish Island is multistage and complex, with at least five deformation episodes (Lamb, 2000; Schermer et al., 2007). At least two folding events that predated the development of kink bands were accompanied by development of veins and pressure solution cleavages whose orientations and fabric associations are distinct from later kink bands and kink-related pressure solution seams; the folding events were followed by multiple faulting events and vein development during a period of extension (Lamb, 2000; Schermer et al., 2007). The most recent deformation events include development of kink folds, strike-slip faults, and possibly open folding of all preexisting structures. Field observations and previous thin section analyses by Lamb (2000) suggest that kink folding occurred after all fabric-forming events: kink bands are notably absent in areas with strongly developed F2 folds or V2 veins, and both the S1 and S2 cleavages are kinked. Although some post-kinking vein development is possible, no penetrative deformation has occurred since kink bands developed (Lamb, 2000; Dunham, 2010).

## 3. Kink bands in outcrop

### 3.1. Field observations and measurements

Kink bands are well exposed in coastal outcrops and a reclaimed quarry along the northern point of Samish Island (Fig. 2). Kink bands range from several millimeters to several centimeters wide and are separated by up to tens of centimeters (Fig. 3a); these kink bands are similar in size to those measured by Verbeek (1978), Kirker and McClelland (1997), Martín-Hernández et al. (2005), and Debacker et al. (2008), and occur in low-grade rocks similar to those analyzed by Anderson and Morris (2004) and Martín-Hernández et al. (2005). The kink bands are dominantly monoclinal and many have anastomosing trends across the foliation surface (Fig. 3a). The curving and anastomosing trends of the kink bands are common throughout the field area, and complex patterns are present on the foliation surface (Dunham, 2010). For microstructures and AMS fabrics in this study, care was taken to select samples in which the kink bands have straight boundaries. Conjugate kink bands are very rare, occurring in only a few locations. Shortening accommodated by individual kink bands on Samish Island ranges from 0.1% to 10% but is less than 3% for the majority of kink bands; shortening across kink band outcrops up to 1.3 m wide is generally less than 5% (Dunham, 2010).

Sigmoidal veins and triangular voids are closely associated with kink bands. Veins parallel to the foliation are kinked in many places (Fig. 3b), and some veins cut through kink bands in others. Small (1–2 cm long, millimeters wide) sigmoidal veins are arranged en echelon across kink band boundaries in several locations; in some places, small triangular voids along the boundaries are connected through the kink band by thin veins that cross the kinked foliation at low angles. Triangular voids filled with quartz along kink band boundaries are also common regardless of other vein fill (Fig. 3b and examples below).

Field measurements of kink band parameters show a wide variation in kink band geometries (Fig. 4). Kink band spacing ranges from <1 cm to >50 cm but is most commonly 3–4 cm ($N = 222$). Kinked widths are commonly 0.2–0.6 cm but range up to 2 cm ($N = 214$); plan widths are slightly narrower but have a similar range. The angular relationships of the kink angles also vary: the external angle ($\alpha$) is generally between 60° and 80°, and the internal kink angle ($\beta$) has an even wider range of 55-90° ($N = 187$ for both). Kink bands within individual outcrops do not necessarily have the same kink angles as adjacent kink bands. Kink bands with $\beta = \alpha$ ($\beta/\alpha = 1 \pm 0.1$, allowing for measurement errors of 5°) are most common ($N = 75$), but kink bands with $\beta > \alpha$ ($N = 52$) and $\beta < \alpha$ ($N = 68$) are also common. The rotation angle ($\kappa$) through which the foliation has been kinked averages 36° but ranges from <10° to 70° ($N = 187$).

There are some differences in the characteristics of the three populations of kink bands defined by $\beta/\alpha$ relationships. All three types of kink bands have similar distributions of kinked widths and average spacing, though kink bands with $\beta \neq \alpha$ have higher plan widths than those where $\beta = \alpha$ (Fig. 4). All three types also show Gaussian distributions of the angles $\alpha$, $\beta$, and $\kappa$ (Fig. 4). However, $\alpha$ is significantly lower and $\beta$ significantly higher for kink bands where $\beta > \alpha$ than for kink bands where $\beta = \alpha$; the opposite is observed for kink bands where $\beta < \alpha$ (Fig. 4d, e, and Fig. 5). Because the angles can vary independently, this need not necessarily be true. The distribution of the rotation angle ($\kappa$) is similar for kink bands with $\beta = \alpha$ and $\beta < \alpha$, concentrated between 30° and 50°; however, $\kappa$ is lower for kink bands where $\beta > \alpha$, between 10° and 30° (Fig. 4f and Fig. 5).

### 3.2. Interpretation of field observations

The geometry of kink bands observed on Samish Island can in principle give insight into the kinematic mechanism of kink band formation there. For example, in the idealized models, $\beta = \alpha$ at all

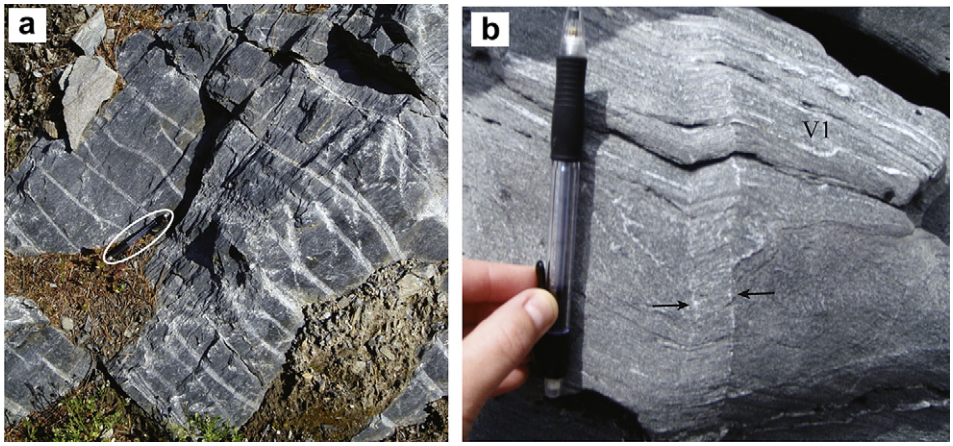


**Fig. 3.** Field photographs of kink bands on Samish Island. (a) A section of outcrop showing a sequence of relatively evenly spaced kink bands; circled is a pencil for scale. (b) A kink band deforming V1 veins parallel to the foliation; arrows denote small quartz-filled voids along the kink band boundaries.

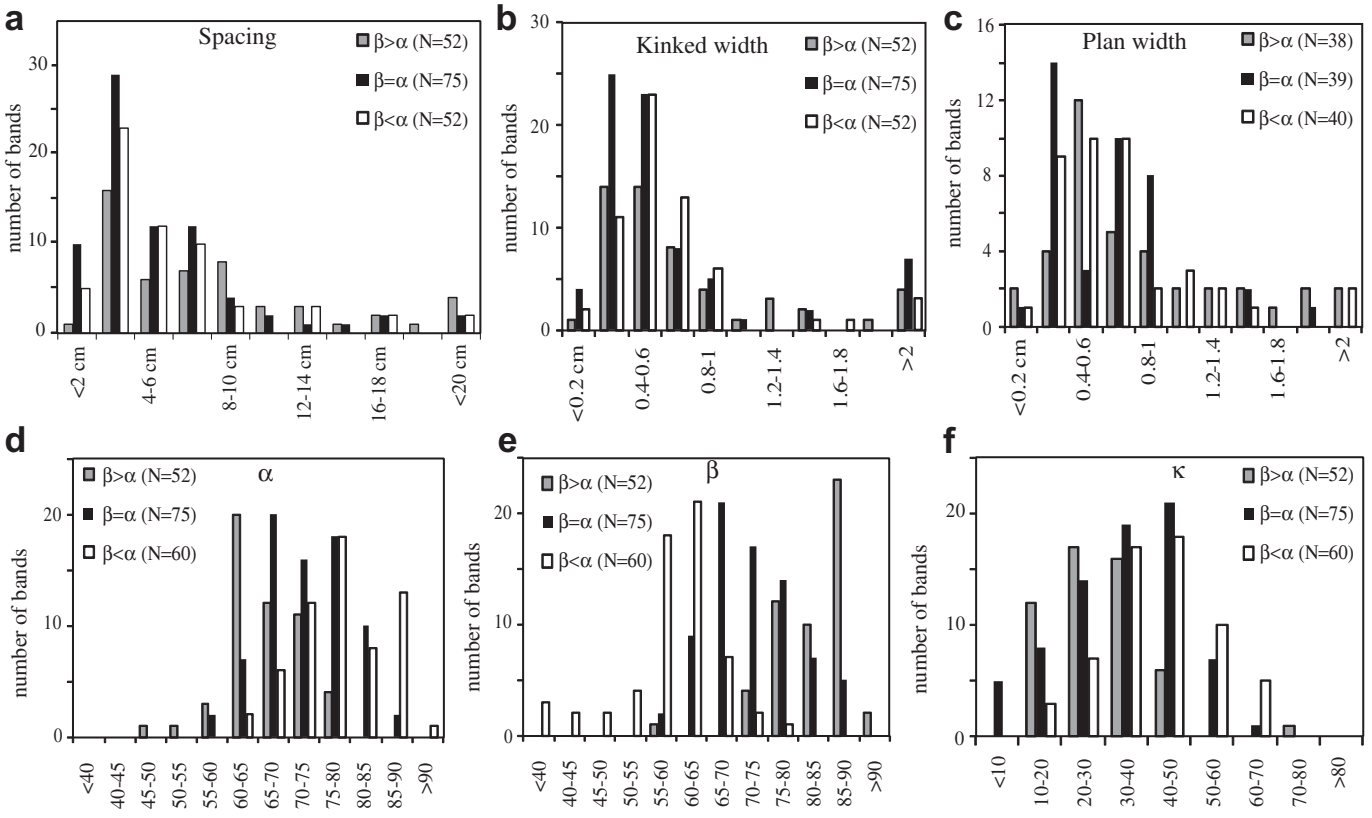


**Fig. 4.** Histograms of kink band parameters measured in the field. Kink bands are separated into three groups based on the angular relationship between α and β (see Fig. 1 for definitions). Totals vary for each group because not all parameters were measureable for all kink bands. (a) Spacing between adjacent kink bands, measured parallel to the external foliation, (b) kinked width, (c) plan width, (d) angle α, (e) angle β, (f) angle κ.

times for mobile-hinge kinking, and α is independent of β in fixed-hinge kinking (Verbeek, 1978). Kink bands from Samish Island have a range of α and β relationships. From this we might conclude that fixed-hinge kinking is dominant; however, it is possible for the angles to be modified by subsequent layer-parallel slip (rotation), and so by themselves are not diagnostic (Stewart and Alvarez, 1991). The wide ranges of observed α and κ suggest that progressive rotation occurred inside and possibly outside the kink bands. In the fixed-hinge kinking model, κ increases progressively, β and plan width both decrease significantly, and kinked width and α (if no external rotation) remain unchanged. In the classic model of mobile-hinge kinking, the value for κ is constant. In a hybrid model of mobile-hinge kinking with progressive internal rotation, κ should increase while both α and β decrease at the same rate, and kinked width should increase (by adding new material) while plan width may decrease slightly (due to shortening). For kink bands on Samish Island, α and β both decrease with increasing rotation (Fig. 5); however, the two angles do not decrease at the same rate, suggesting independence. The similar distribution of κ for kink bands where $\beta = \alpha$ and $\beta < \alpha$ suggests that once a kink band reaches $\beta = \alpha$ it locks, and only the external foliation continues to rotate to accommodate further shortening.

The observed range of widths and the relationships between angles and width do not clearly distinguish between the two

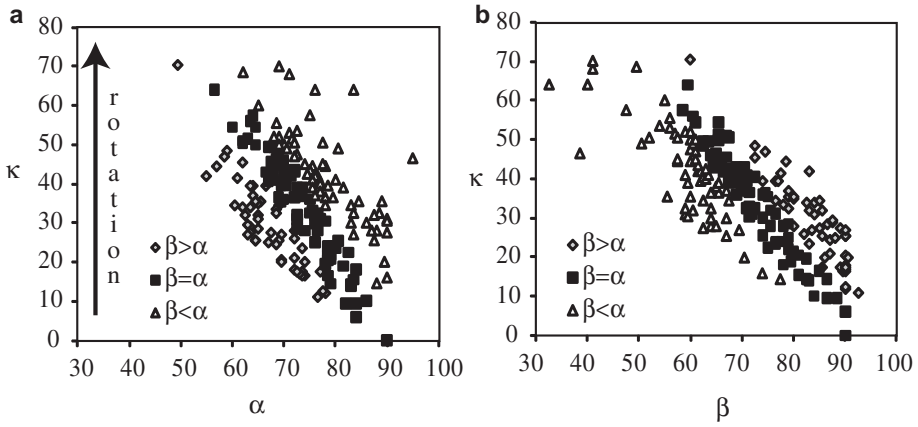


**Fig. 5.** Scatter plots of angular parameters for 217 kink bands classified by β/α ratios. (a) α vs. κ showing decreasing α with increasing κ; (b) β vs. κ showing decreasing β with increasing κ. $N = 52$ for $\beta > \alpha$; $n = 75$ for $\beta = \alpha$; $n = 60$ for $\beta < \alpha$.

models. The kinked width distribution shows similar ranges and patterns for all three subsets, which suggests that the width of the kinked limb is arbitrary and may be set from the initiation of the kink band. Judging by the peak in the histograms, plan width may decrease slightly from $\beta>\alpha$ to $\beta = \alpha$, consistent with rotation of a kinked limb with fixed width; however, $\beta<\alpha$ kink bands have greater plan and kinked widths than $\beta>\alpha$ kink bands, which suggests that kink bands may widen once they lock. Thus, both fixed-hinge and mobile-hinge kinking may operate: as a kink band accommodates shortening by rotation, the kinked width remains constant but the plan width decreases until the kink band locks at $\beta = \alpha$ (fixed-hinge kinking); further deformation is accommodated by lateral migration of the kink band boundaries (mobile-hinge kinking) and/or rotation of the foliation outside the kink band.

Triangular deposits of quartz and/or calcite along kink band boundaries and in sigmoidal veins within the kink bands indicate dilation during kinking. During rotation of the internal foliation of a fixed width, dilation must occur within the kink band, separating the foliation and creating triangular voids along the boundaries (Verbeek, 1978); both triangular voids and internal veins are seen on Samish Island. The sigmoidal veins, in most cases, are not parallel to the kinked foliation but cross it at low angles.

The field-documented geometric relationships alone cannot conclusively distinguish between fixed- and mobile-hinge kinking. The observations do require progressive internal rotation and dilation within the kink bands, whether the kink band boundaries were fixed or migrating. We turn to microstructures and magnetic fabrics to provide more information.

## 4. Microstructures

### 4.1. Basic lithology and fabrics

Thin sections were prepared perpendicular to both the foliation and the kink band hinge lines for 14 kink bands. The dominant mineral phases identified in thin section are quartz, feldspar, white mica, and actinolite, with minor calcite, chlorite, and opaques. Lamb (2000) also identified pumpellyite and epidote, and based on the occurrence of actinolite and pumpellyite determined metamorphic conditions of 200–350 °C and 2–7 kbar. Grain size is generally very fine, with the coarsest grains up to 2 mm in some samples. The main foliation is defined by layers of recrystallized quartz with a grain-shape or aggregate-shape preferred orientation, alternating with concentrations of aligned mica and weakly aligned actinolite laths (Fig. 6a). The foliation is weakest in the coarser-grained samples, defined by wispy mica and anastomosing pressure solution seams around quartz grains. As the proportion of mica increases, the foliation is better developed and more clearly defined by a ~2:1 ratio of thicker quartz (1–2 mm) to thinner mica (0.5 mm) layers.

Evidence for pre-kinking pressure solution within the bulk rock is clearly seen in most samples. Dark pressure solution seams are roughly parallel to the foliation in most rocks (Fig. 6a), associated with the mica-rich horizons and found both inside and outside kink bands; Lamb (2000) interpreted these seams as evidence for a second foliation-forming event well before kink bands developed. A different set of discontinuous seams oriented about 30° from the foliation anastomose around quartz grains in several samples and have no clear relationship with kink bands in those rocks; the

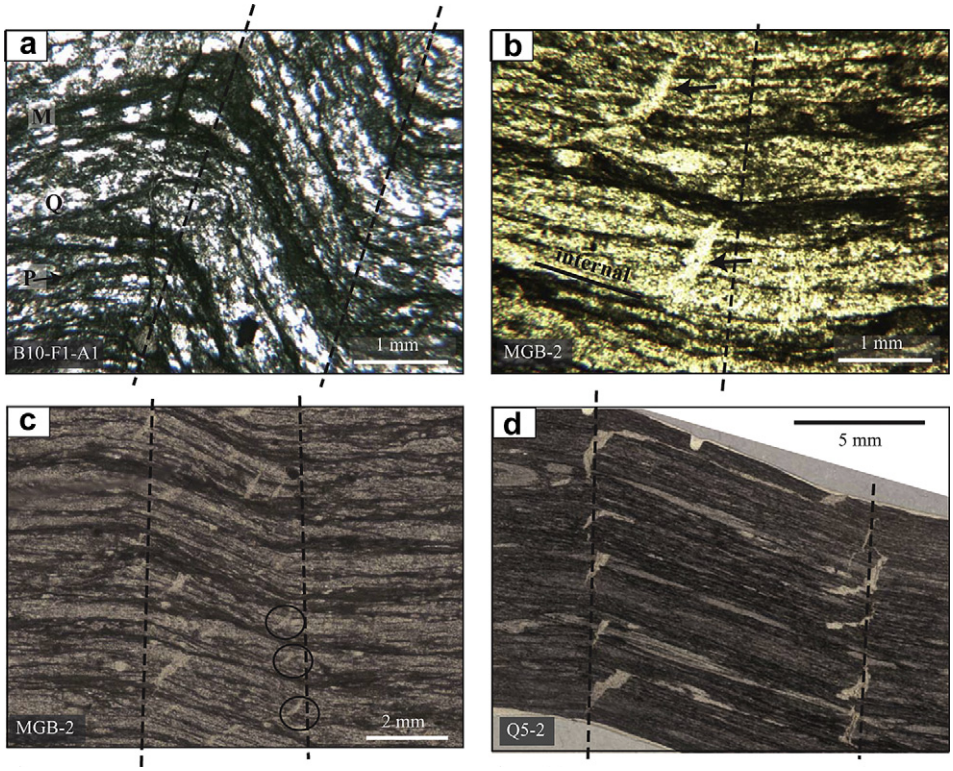


**Fig. 6.** Micro-scale features of kink bands in thin section. Kink band boundaries are shown by dashed black lines. (a) An angular kink band in crossed polars. Both the mica (M; dark) and quartz (Q; light) horizons bend sharply at the boundary. A pre-kinking pressure solution seam (P) is visible parallel to the main foliation. (b) A rounded kink band hinge in plane light; note the triangular gashes filled with quartz inside the boundary (arrows). (c) Small, roughly triangular gashes (several are circled) along a kink band boundary; most occur at the boundary itself, but several are inside the kink band. (d) Large, well-developed triangular hinge voids along the boundaries of a very wide kink band. Note that the bases of many voids extend into the kink band as layer-parallel veins.

orientation and expression of this set of seams is consistent with Lamb (2000) interpretation of a third deformation sequence, also pre-kinking. Both sets of pressure solution seams consist mainly of dark insoluble residues and minor mica.

### 4.2. Kink bands

In thin section, we measured: kink angles α, β, and κ; width of the kinked limb along its trace; thickness of the foliation inside and outside the kink band (Fig. 1); we also recorded the geometry and shape of the hinges and the presence of voids, gashes, or veins associated with the kink bands (Table 1). The foliation thickness was taken as the average spacing between mica horizons; for sample B1-1, the foliation is defined by pressure solution seams bounding quartz grains in single layers. The size of voids was measured as the median width perpendicular to median line of the void.

Common elements among the majority of kink bands include: relatively consistent spacing of foliation layers inside and outside kink bands; uniform extinction of micas inside kink bands; sharp to rounded hinges across which the foliation is continuous (Fig. 6a, b); and quartz- or calcite-filled voids along kink band boundaries (Fig. 6b–d). The bulk rock is similar in composition and grain size inside and outside the kink bands. Grains inside kink bands are generally not bent or broken, and there are no clear strain markers. Kink band boundaries are generally sharper and better defined in more micaceous samples (Fig. 6a), whereas rounded, diffuse kink band boundaries are common in more quartz-rich and/or coarser-grained samples (Fig. 6b).

Quartz- or calcite-filled voids and/or veins are commonly associated with kink bands that display unequal kink angles β and α (6 out of 10 kink bands with $\beta \neq \alpha$); voids spaces are rarer in kink bands where $\beta = \alpha$ (1 out of 4 with $\beta = \alpha$). Voids range in size from small, elongate en-echelon gashes along the hinges (Fig. 6c) to large, well-developed triangular spaces (Fig. 6d). Larger spaces occur in wider kink bands with very large β values (Table 1). Voids are not observed in very narrow kink bands (e.g. less than 2 mm kinked width). The quartz or calcite crystals filling the void spaces are generally much coarser than in the bulk rock and show little evidence of recrystallization or deformation. Characteristics of the void fill are clearly visible in the large voids of sample Q5-2 (Fig. 6d). Quartz adjacent to the external foliation is fibrous and elongate parallel to the external foliation (Fig. 7a); grains are larger and more polygonal in the center of the void. Quartz fibers on the inside edges of the voids are rare but, where visible, are parallel to the kinked foliation. The presence of quartz fibers that are connected to the bulk rock on both sides is consistent with syntaxial growth of the void fill. In many examples, the voids extend into the kinked rock as veins at low angles to the foliation (Fig. 7b). Several of the triangular voids at the boundary of the same kink band are distinctly offset in a dextral stepwise pattern parallel to the kinked foliation (Fig. 8a); this stepwise offset pattern is also seen in smaller voids in at least one other kink band. The edges of larger voids in several other kink bands are ragged due to very small-scale interfingering of mica grains with the fine-grained quartz at the rims (Fig. 8b).

Pressure solution inside kink bands is evident only in those kink bands for which α and β are equal. In these kink bands, pressure solution seams are concentrated within the kink bands themselves and do not extend into the rock outside the kink band (Fig. 9). Pressure solution seams are oblique to the kink boundaries and persist through the full width of the kink band, not just in the hinges as observed by Stewart and Alvarez (1991). Where the seams coincide with the boundaries, the hinges are sharper than at those segments without coincident pressure solution. The seams are more closely spaced in more micaceous, fine-grained rocks. Clear offsets are seen in the mica layers across the seams; the magnitude of apparent displacement is varied even within individual kink bands. Pressure solution seams are also visible along the hinges of several other kink bands (Table 1), but these seams are confined to the hinge zones and are isolated and discontinuous.

### 4.3. Interpretation of kink bands in thin section

We interpret these observations to indicate that interlayer slip and pressure solution both operated during kinking. Interlayer slip is expected in kink bands forming via rotation with either mobile or fixed hinges, and in the case of kink bands from Samish Island is the

**Table 1**
Kink band parameters measured in thin section.

| Kink band | α | β | κ | KW[a] | Mica/quartz ratio | Foliation spacing[b] | Hinges | Voids (widths, mm) | PS[c] |
|---|---|---|---|---|---|---|---|---|---|
| β>α | | | | | | | | | |
| Q5-2-A1-1 | 78 | 97 | 8 | 17 | Q << M | 0.4 mm | Sharp | 1.2 | – |
| B10-F1-A2-1 | 72 | 91 | 17 | 7 | Q ~ M | 0.5 mm | Rounded | 0.1 | – |
| B13-F3-A1-2 | 60 | 85 | 35 | 10 | Q > M | 1–2 mm | Sharp | 0.6 | – |
| B10-F1-A1-1 | 65 | 81 | 34 | 4.5 | Q ~ M | 0.2–1 mm | Rounded, sheared | 0.3 | – |
| B13-F3-A1-1 | 60 | 74 | 46 | 1 | Q > M | 1–2 mm | Sharp | – | H |
| B13-F1-A2-1 | 60 | 70 | 50 | 2 | Q > M | 1 mm | Sharp | – | H |
| Q4-4-A1-1[e] | 68 | 86 | 26 | ≥6[d] | Q > M | 1 mm | Sharp, sheared | – | H |
| β = α[f] | | | | | | | | | |
| B1-1-A1-1 | 63 | 65 | 52 | 8 | Q >> M | ~1 mm | Rounded, diffuse | 0.2 | 34° |
| B13-F2-A1-1 | 60 | 60 | 60 | 5.5 | Q ~ M | 0.5 mm | Subrounded | – | 10° |
| B13-F2-A3-1 | 60 | 60 | 60 | 4 | Q ~ M | 0.5 mm | Subrounded | – | 10° |
| Q4-2-A1-1 | 67 | 70 | 43 | ≥8 | Q > M | 1 mm | Subrounded | – | 25° |
| β<α | | | | | | | | | |
| MGB2-A1-1 | 88 | 68 | 24 | 4 | Q > M | 0.5–1 mm | Rounded | 0.3 | – |
| B13-F1-A1-1 | 81 | 67 | 32 | 2 | Q > M | 1 mm | Sharp | – | – |
| Q4a-1-A1-1[e] | 75 | 70 | 35 | 4 | Q > M | 1 mm | Rounded | 0.3 | – |

[a] Kinked width (mm).
[b] Foliation spacing measured as average quartz layer thickness between mica layers or pressure solution seams.
[c] Pressure solution within kink bands and angle with kink band hinge; H indicates seams along hinge only.
[d] Minimum width only; kink band is incomplete in thin section (only one hinge visible).
[e] Also analyzed for AMS.
[f] $\beta = \alpha$ is assigned when $|\beta - \alpha| < 5°$.

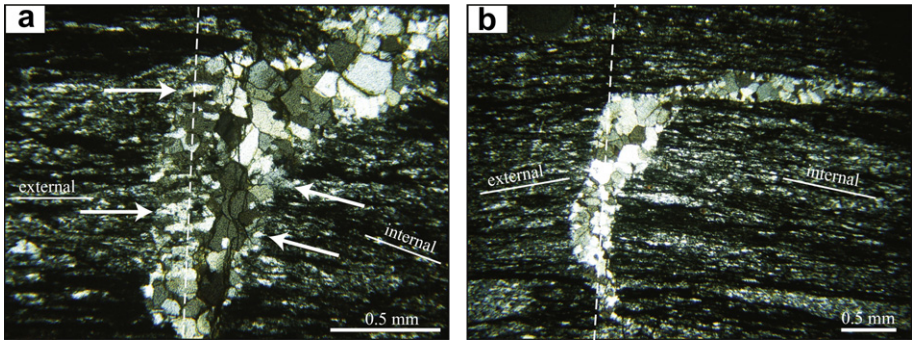


**Fig. 7.** Photomicrographs in crossed polars showing details of quartz-filled triangular void spaces; white dashed lines mark kink band boundary. (a) Quartz fibers on both sides of the void (arrows), adjacent to wall material, are elongate and track the first opening phase of the void; quartz grains on the inside of the void are larger and polygonal. The fractures through the center of the void are part of a through-going fracture along the kink band boundary that appears to post-date kink formation. (b) Wide view of a single triangular void in the same kink band whose base extends into the kink band as a vein. The vein is filled with similarly polygonal quartz as the body of the void, and cuts the kinked foliation at a low angle.

dominant grain-scale mechanism of kinking. The protrusion of mica grains into the void spaces along kink band boundaries suggest interlayer slip during kinking: as the kinked foliation rotated and void spaces opened in the hinges, slip along the foliation caused mica grains to protrude into the void spaces. Syn-kinking infilling of those voids trapped the mica grains, resulting in ragged edges inside the kink band (Fig. 8b). These mica protrusions do not occur on every mica horizon; thus, slip may be localized to spaced horizons within the kink bands. One example of protrusion of external micas into the outside edges of void spaces was also observed; thus we observe direct evidence for interlayer slip outside the kink band.

Pressure solution also accommodated shortening inside kink bands, but did not operate within all kink bands. The low, oblique angles between the pressure solution seams inside kink bands and the kink band boundaries are consistent with pressure solution during kink band formation, controlled by the same strain field. The monoclinal pattern of kink bands on Samish Island requires a principal shortening direction oblique to the kink band boundaries, and the sense of obliquity (i.e. upper left to lower right for dextral kink bands such as that in Fig. 9) is consistent with the orientation of pressure solution seams inside the kink bands. The lack of similarly oriented pressure solution seams outside any of the analyzed kink bands also suggests that the timing and localization of pressure solution was controlled by kinking. The association of internal pressure solution with only those kink bands where $\beta = \alpha$, indicates that rotation could no longer accommodate shortening because the kink bands were indeed "locked;" further shortening was accommodated by pressure solution and/or rotation of the external foliation.

The stair-step geometry of larger voids provides further evidence for rotation and interlayer slip. The void fill is not deformed or fractured along the "step" planes: the geometry represents the initial form of the void. The sense of step of each void is consistently toward the interior of the kink band, beginning from the triangular tip of the void. The voids in sample Q5-2 (Fig. 6d and Fig. 8a) apparently initiated as a series of fractures at low angles to the kink-band boundary, connected by planes of sinistral slip (and opening) parallel to the foliation. Fractures appear to dominate in the quartz-rich layers. The connected voids accommodate the bending strains at the kink band boundary, facilitating internal rotation. This "rip and slip" mechanism divides the kink band into macro-packets of quartz and mica, separated by horizons of greater slip and expansion, frequently also occupied by veins and bracketed on either side by voids (Fig. 6d and Fig. 7b).

Microstructural and field observations are consistent with the fixed-hinge model of kinking, though elements of mobile-hinge kinking cannot be completely dismissed. The ubiquity of void spaces within kink bands and the presence of kink bands with unequal angles $\alpha$ and $\beta$ (Table 1) are both consistent with fixed-hinge rotational kinking. Previous workers (e.g. Anderson, 1964; Ramsay, 1967; Verbeek, 1978; Debacker et al., 2008) have shown that dilation within a kink band is at a maximum when $\beta = 90^\circ$ and $\beta > \alpha$. In Samish Island rocks, voids are more common in kink bands where $\beta > \alpha$, and the largest voids are seen in wider kink bands with $\beta$ values close to or greater than 90° (e.g. kink bands in

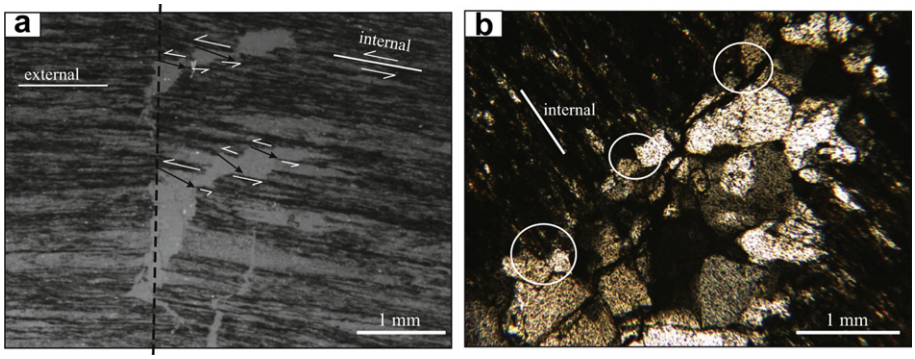


**Fig. 8.** Stair-step voids along the hinges of the same kink band shown in Fig. 6d and Fig. 7. White arrows show the relative motion of the foliated rock; black arrows show displacement vectors of points on either side of the void. The kink band boundary is shown by the dashed black line. (b) Photomicrograph in crossed polars of mica grains protruding from the kinked zone into a large void space (circles). The kink band boundary passes through the void.

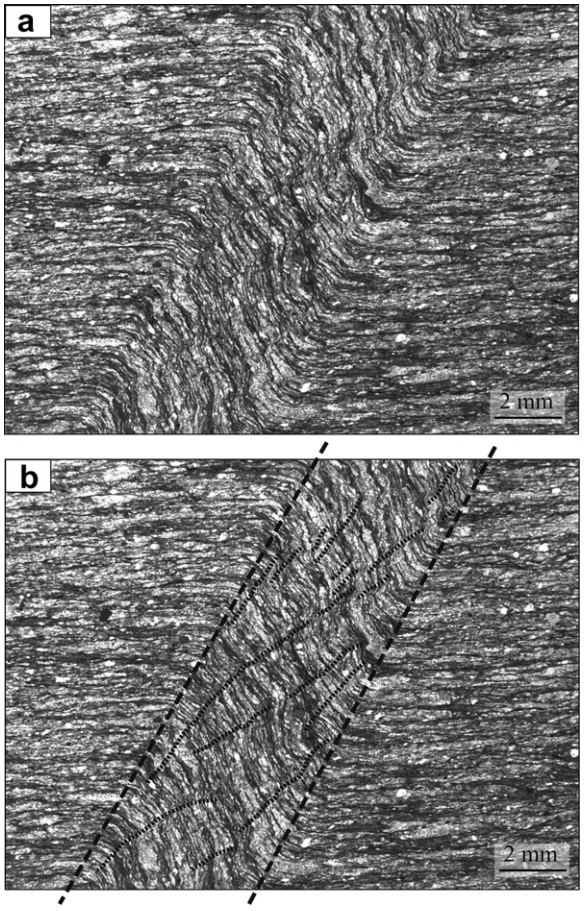


**Fig. 9.** Pressure solution seams confined to a kink band where $\beta = \alpha$. (a) Raw photograph in transmitted light; (b) pressure solution seams inside kink band traced by dotted lines. Dashed bold lines show the kink band boundaries. Note that none of the seams cross the kink band boundaries, and no seams of this orientation are visible outside the kink band.

samples Q5-2 and B13-F3; Table 1). The transition from fibrous to polygonal quartz growths inside the larger voids (Fig. 7a) suggests multiple opening phases: opening during the first phase may have been very small, promoting fibrous growth; as rotation progressed, the space widened and larger polygonal grains precipitated. Triangular voids along kink band boundaries and veins extending from those voids into the kinked rock both indicate dilation inside the kink bands during development of the folds, which is required by the fixed-hinge model (Anderson, 1964; Verbeek, 1978). Fixed-hinge kinking is also consistent with locking of the kink bands at $\beta = \alpha$ and the need for a different mechanism (e.g. pressure solution or external slip/rotation) to accommodate further shortening.

There is some evidence to suggest mobile-hinge kinking may have played a role in the development of these kink bands, possibly in later modification of the kink hinges. Discontinuous pressure solution seams along some kink band hinges (but not inside the kink bands) may have served to tighten the kink hinges, similar to observations made by Stewart and Alvarez (1991) in mobile-hinge kink bands. Paterson and Weiss (1966) observed broken quartz grains inside experimentally-deformed phyllites and interpreted these fractures to mark the passage of migrating boundaries through the grains: as the quartz grain was folded and then unbent, closely spaced fractures developed within the crystal Such broken grains are notably absent in kink bands from Samish Island.

## 5. Magnetic fabric

### 5.1. Background

Anisotropy of magnetic susceptibility (AMS) is controlled by the crystallographic orientation and shape of minerals within a rock. In foliated rocks, the iron-bearing phyllosilicates that define the foliation typically dominate the paramagnetic susceptibility signal (Parés and van der Pluijm, 2002). Other iron-bearing tabular or elongate minerals may contribute to that signal, and ferrimagnetic grains such as magnetite may add a ferrimagnetic susceptibility as well (Parés and van der Pluijm, 2002). All of the minerals in a rock contribute to its bulk susceptibility (Tarling and Hrouda, 1993), and understanding the distribution and crystallographic orientations of such minerals is important to interpreting the magnetic fabric of a rock. The AMS of a sample can be described by a $3 \times 3$ matrix whose eigenvalues and eigenvectors provide the magnitudes and orientations of the three principal susceptibilities ($k_{max}$, $k_{int}$, $k_{min}$) that define the AMS ellipsoid. This AMS ellipsoid can be presented and evaluated using the same geometric methods as used for the strain ellipsoid. The shape of the AMS ellipsoid can be described using ratios of the principal susceptibilities: the lineation (L) parameter, or $k_{max}/k_{int}$, and the foliation (F) parameter, or $k_{int}/k_{min}$ (Tarling and Hrouda, 1993). These two ratios can be plotted on a Flinn diagram to portray the shape of the ellipsoid and therefore the dominant fabric of the rock as prolate (elongate; $L > F$), oblate (flattened; $L < F$), or triaxial ($L = F$). Comparing the orientation of the ellipsoid with structural orientations can associate a magnetic fabric with a deformation fabric (e.g. Hrouda, 1978; Parés and van der Pluijm, 2002).

### 5.2. Methodology

Three block samples from the quarry on Samish Island with wide, well-expressed kink bands were selected for AMS analyses. Cores 1.25 cm in diameter were drilled from material both inside and outside major kink bands and then cut into ~1 cm long specimens; while these are about one tenth the volume of standard specimens used for paleomagnetic studies, they are in turn about 3.5 times the size of chips used successfully by Kirker and McClelland (1997). Thin sections were cut from adjacent material in order to assess the occurrence of pressure solution in the kink bands and to confirm the mineralogy of the rocks. Susceptibilities of the specimens in a low magnetic field were measured in the Pacific Northwest Paleomagnetism Lab at Western Washington University using a KLY3-S Kappabridge. The operating program measures each specimen in three orientations, obtaining the susceptibility differences in three orthogonal planes and the susceptibility in one direction. Output is mean or normalized susceptibility and matrix elements for the AMS from which the principal susceptibilities and directions are calculated. Susceptibilities were adjusted to a common specimen volume using specimen mass and estimated density (Table 2). Although care was taken to include as little material as possible from hinges or from outside the kink bands in the kink band cores, most specimens from these cores included material from outside, the volume of which was geometrically estimated. We used matrix algebra (Fig. 10) to subtract the outside contribution to the kink specimens (range: 0%–76%; average: 42%) in order to calculate the AMS of pure kink material. The expected (rigidly rotated) fabric was calculated using the average AMS of all "outside" specimens in a sample and the measured angle $\kappa$ for each kink (Table 2). Observed fabrics from kinks are the averages of two specimens, except for Q4-4 kink 1, for which we have only one specimen. We used programs by Tauxe

**Table 2**
AMS results and related parameters.

| Sample and zone[a] | Bulk susceptibility[b] | % change[c] | F | L | α | β | κ | Type of kink band |
|---|---|---|---|---|---|---|---|---|
| Q4a-1 outside | 2.5675E-04 | – | 1.06 | 1.09 | – | – | – | – |
| Q4a-1 kink 1 | 2.2066E-04 | −14.1% | 1.09 | 1.13 | 75 | 67 | 38 | β<α |
| Q4-2 outside | 2.7890E-04 | – | 1.06 | 1.09 | – | – | – | – |
| Q4-2 kink 1 | 2.7675E-04 | −0.8% | 1.05 | 1.09 | 67.5 | 81 | 31.5 | β>α |
| Q4-2-kink 3 | 2.5892E-04 | −7.2% | 1.05 | 1.03 | 75 | 77.5 | 27.5 | β = α |
| Q4-2 kink 4 | 2.5724E-04 | −7.8% | 1.05 | 1.09 | 70 | 70 | 40 | β = α |
| Q4-4 outside | 2.5115E-04 | – | 1.05 | 1.10 | – | – | – | – |
| Q4-4 kink 1 | 2.5536E-04 | 1.7% | 1.04 | 1.10 | 67.5 | 73 | 39.5 | β>α |
| Q4-4 kink 2 | 2.9326E-04 | 16.8% | 1.04 | 1.06 | 68 | 80 | 32 | β>α |

[a] "Outside" values are the average of specimens of foliation outside the kink bands, $N = 2–6$.
[b] Average susceptibility for all specimens from each zone.
[c] Change in susceptibility, calculated as [(kink-outside)/outside] × 100.

(1998) to rotate AMS matrices, convert between matrix and eigenvalue-eigenvector descriptions, and plot the data.

To evaluate magnetic mineralogy, the magnetic moment versus magnetic field of select specimens was measured parallel to the outside (mineral) lineation using a Princeton Measurements vibrating sample magnetometer (VSM). Data were normalized by mass so specimens from both outside and inside kink bands could be compared.

### 5.3. Results

#### 5.3.1. Magnetic mineralogy

The raw hysteresis curves appear as single lines with positive slopes (Fig. 11), indicating that the bulk sample magnetic signal is paramagnetic. Correction of the raw data for the high field slope leaves a small S-shaped curve consistent with a very small contribution from ferromagnetic phases. Both the internal and external material produce similar raw and corrected hysteresis curves, with the corrected curves plotting on top of each other. The slightly lower slope for material inside a kink band is consistent with dilation and infilling of voids with diamagnetic phases (e.g. quartz), but the slope could also be lower in the kink specimens because lineation in the kink bands was not parallel to the magnetic field.

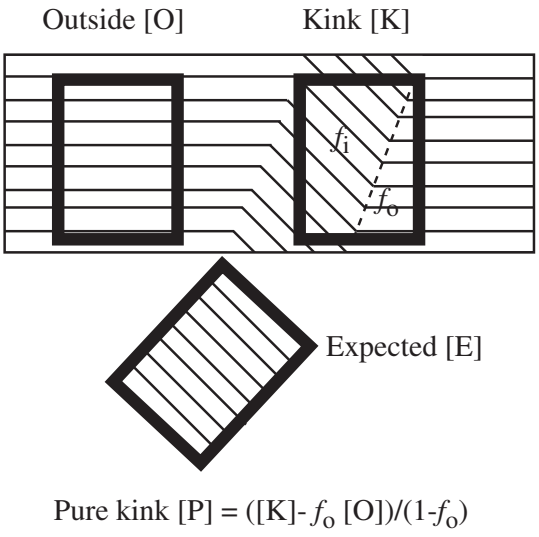


**Fig. 10.** Cartoon showing how the susceptibility ellipsoid of pure [P] kink material was determined from measurements of outside material [O] and kink specimens [K] that were contaminated with $f_o$ fraction of outside material. Expected [E] is [O] rotated by the angle κ about the kink hinge line (see Fig. 1 for κ).

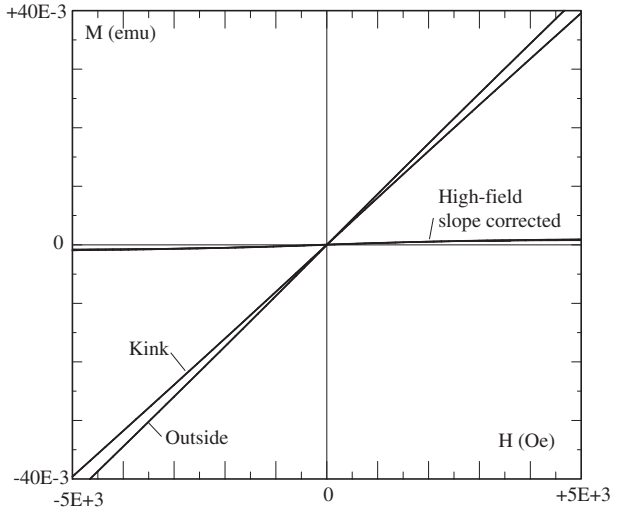


**Fig. 11.** Hysteresis results for sample Q4-2, plotting applied magnetic field (H) vs. induced magnetic moment (M). The outside and kink fabrics both produce visually straight lines with positive slopes, indicating dominance of paramagnetic minerals. After correction for the high field slope, the M-H data trace narrow loops for both the outside and kink fabrics. These plot on top of each other, indicating that both have similar, very small quantities of a ferromagnetic mineral.

Regardless, the difference is small compared to other uncertainties, and thus we assume that there is negligible mineralogic difference between the two zones; this is consistent with thin section observations from the same samples.

#### 5.3.2. Anisotropy of magnetic susceptibility (AMS)

The AMS results are shown in Fig. 12 as equal area plots of the principal susceptibility axes; for ease of comparison, all data are plotted with the foliation outside the kink band horizontal, outside mineral lineation E-W, and kink bands stepping down to the right. We used mineral lineation E-W instead of kink hinge-lines N–S (e.g. Kirker and McClelland, 1997) because the lineation orientation is consistent across the outcrops, whereas kink hinge lines have various attitudes. The orientations of the AMS ellipsoids in Fig. 12 reflect the structural elements of the rocks. For specimens outside the kink bands (Fig. 12a), $k_{max}$ and $k_{int}$ lie in the plane of the foliation, with $k_{max}$ aligned with the lineation in each sample; $k_{min}$ clusters near the pole to the foliation. That $k_{min}$ is not precisely perpendicular to the foliation likely is due to small errors in orientation of cores relative to the imperfectly planar foliation; the same can be said for the imperfect parallelism of $k_{max}$ and the lineation. However, only comparisons between samples are affected by this; comparisons within samples are not because they use the same frame of reference. The maximum and intermediate axes align well with and perpendicular to the macroscopic lineation, respectively.

Comparing the fabrics observed within the kink bands with those expected from rigid rotation of the outside fabric shows significant differences (Fig. 12b). The magnetic lineation ($k_{max}$) is rotated in the plane of the foliation 20° or more relative to the expected direction and reoriented more normal to the kink hinge line. In most of the samples, $k_{min}$ plunges 5–10° shallower than expected, representing a steepening of the magnetic foliation relative to the mineral foliation (also seen in steepened plunges of $k_{max}$ and $k_{int}$).

The shape factors of the anisotropy ellipsoids and susceptibilities for each specimen are shown in Fig. 13 and listed in Table 2. The AMS ellipsoids for outside specimens are prolate, consistent with a well-defined lineation (Fig. 13a). The AMS ellipsoid shapes in

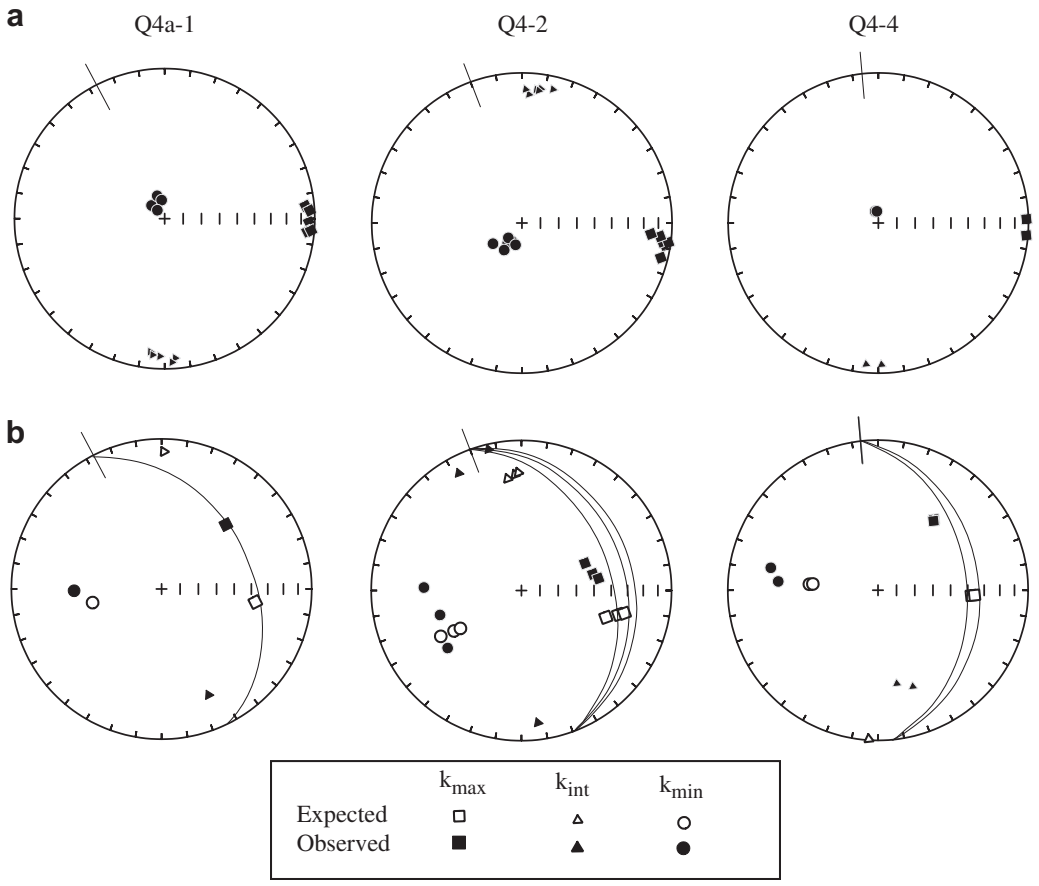


**Fig. 12.** Equal area lower hemisphere plots showing the orientations of the principal susceptibility axes for (a) outside, (b) expected (mean outside eigenvectors rotated by κ separately for each kink) and pure kink (outside contamination removed from observed kink specimens). The outside foliation is horizontal and the mineral lineation oriented E-W in each plot for a common frame of reference; kink hinge line orientations are indicated by long ticks and the kinked foliation for each kink band is shown by great circles.

three of the kink bands are similar to the outside fabric (suggesting little change despite reorientation). The other three kink bands exhibit different behaviors: two remain prolate but have opposite inverse correlations of susceptibility and anisotropy (Q4-4 kink 2 and Q4a-1 kink 1); the third has an oblate fabric with lower anisotropy than outside, but no difference in susceptibility.

### 5.4. Interpretation of AMS

The tight groupings of axes for specimens from outside the kink bands (Fig. 12a) provide visual confirmation of robustness of the data. AMS observations from within the kink bands suggest that a variety of mechanisms may be operating to modify the magnetic

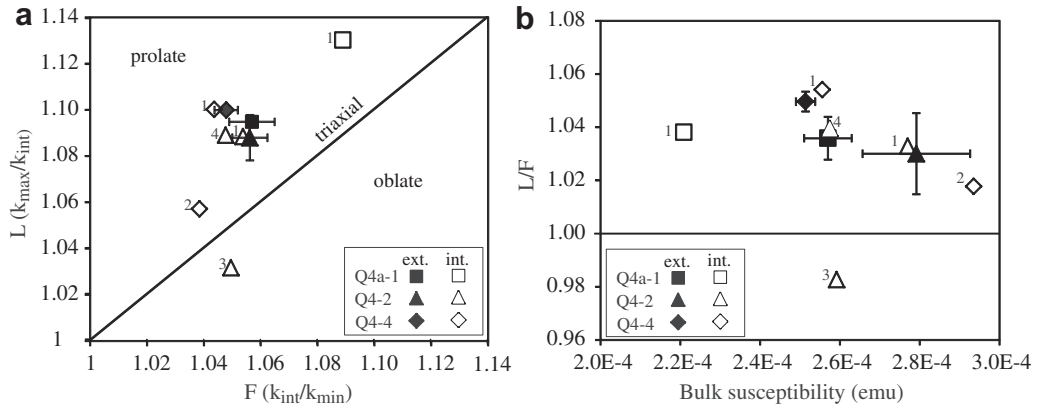


**Fig. 13.** (a) Flinn plot of the shape factors of the AMS ellipsoid for the magnetic fabric outside and inside kink bands (ext. and int., respectively); numbers refer to specific kinks as listed in Table 2 and error bars show the range of values for all outside specimens. The outside fabric is similar for all three samples, plotting in the prolate field. The kink fabrics in three kink bands are not very different from the related outside fabric; however, one kink (Q4a-1 kink 1) shows an increase in anisotropy and two (Q4-2 kink 3 and Q4-4 kink 2) show decreases in anisotropy and prolateness. (b) L/F vs. bulk magnetic susceptibility plot for the same data as (a). The susceptibility inside the kink bands from samples Q4a-1 and Q4-2 is the same as or lower than the outside fabric; the susceptibility increases within kink bands from Q4-4.

fabrics during kinking. The hysteresis results (Fig. 11) demonstrate that iron oxides and sulfides contribute negligibly to the AMS; thus, such mechanisms need involve only the main silicate framework grains.

The similarity of anisotropy and susceptibility in half of the kink bands with outside material is consistent with simple reorientation of outside fabrics (Fig. 13). Disagreement of observed and expected orientations of $k_{max}$ shows that the mechanism is not simple folding around kink hinge lines (Fig. 12b). If kink band formation involves interlayer slip, as we observed above, this process could add a magnetic "stretching" lineation. If this interlayer slip were normal to kink band hinges, the resulting $k_{max}$ lineation would be normal to the kink hinge line (observed in Q4-2). In specimens from rocks Q4a-1 and Q4-4, $k_{max}$ is rotated counterclockwise relative to the expected direction more than can be attributed to hinge-perpendicular interlayer slip alone, but might be explained by oblique slip or later shearing along the kink band boundaries. That the magnetic fabric within the kink band is not more prolate than outside the kink bands weakens the hypothesis of a kinking-produced magnetic lineation.

Different mechanisms must be responsible for changes in susceptibility. The decrease in susceptibility inside kink bands from Q4a-1 and Q4-2 can be explained by dilution of paramagnetic micas through addition of diamagnetic quartz within dilation spaces. Corresponding variations in anisotropy may have been influenced by how much of the added quartz is in the hinges versus veins sub-parallel to the internal foliation. Increased susceptibility observed within Q4-4 kink bands seems to require concentration of paramagnetic minerals. Pressure solution could accomplish this if it selectively removed diamagnetic phases. Insoluble residue in the resulting seams could contribute a new AMS component, reorienting the AMS ellipsoid (i.e. Housen and van der Pluijm, 1991; Kirker and McClelland, 1997). Preferred orientation of these grains at a high angle to foliation (Fig. 9) could lead to destructive interference of the two fabric elements and reduced anisotropy (as in Q4-4 kink 2). Given the range of possibilities, the present AMS study is too small to conclusively identify which mechanisms were responsible for the observed variations in AMS. We have, however, identified mechanisms that should be considered in subsequent investigations.

## 6. Conclusions

Mobile- and fixed-hinge kinking have emerged as the main kinematic models by which we understand kink band formation, but neither model explains all observed kink band geometries (e.g. Hobson, 1973; Verbeek, 1978; Weiss, 1980; Stewart and Alvarez, 1991). In the rocks from Samish Island, the angular relationship $\beta = \alpha$ (expected by mobile-hinge models) is common but not ubiquitous in kink bands, and the significant number of kink bands with $\beta > \alpha$ suggests that fixed-hinge kinking was operative, as this relationship represents early-stages of the fixed-hinge model. The AMS observations require that processes other than simple rigid rotation operated during kink band formation.

There is clear evidence for dilation inside most kink bands, which also supports fixed-hinge kinking. Progressive rotation between fixed limbs results in triangular voids in at the boundaries and layer-parallel expansion inside the kink band (e.g. Verbeek, 1978), both of which are well preserved in the kink bands described in this study. Stair-step void spaces along kink band boundaries are created by connected fractures that accommodate bending at the kink hinge and rotation of the internal foliation. Interlayer slip is evident in thin section from small mica grains protruding into dilation spaces along kink band boundary. The orientations of quartz fibers inside the larger void spaces suggest multiple opening episodes, consistent with progressive rotation of the kinked limb. The interfingering of internal micas with quartz in the hinge void spaces suggests that the void fill was precipitating during kinking, which may have jammed developing kink bands and precluded progression to the "locked" ($\beta = \alpha$) stage, preserving them as immature (see also Verbeek, 1978). Kink bands that did reach the locked stage could no longer rotate, and pressure solution inside the kink bands or slip outside the kink bands allowed further shortening to occur. Minor pressure solution in the hinge region of some kink bands may provide evidence for late-stage hinge tightening and possible migration. The common occurrence of $\beta < \alpha$ suggests slip may have occurred outside the kink bands, as well.

In sum, the observations in this study favor the fixed-hinge kinematic model of kinking for the kink bands on Samish Island, with veining, interlayer slip, and pressure solution as the primary deformation mechanisms. The kink bands in this study accommodate less than 10% shortening and were likely produced during unroofing (Lamb, 2000; Dunham, 2010). Our assessment that fixed-hinge kinking was the dominant kinematic mode is consistent with prior work showing that this mechanism operates at low strains (Stewart and Alvarez, 1991) and low confining pressures (Anderson, 1974). Pilot AMS analyses guide the generation of testable hypotheses regarding the interplay among interlayer slip, void filling by veins, and pressure solution in the development of kink bands by fixed-hinge rotation. Additional microstructural and AMS analyses are required to demonstrate correlations among magnetic signatures and microstructural processes.

## Acknowledgments

We thank: Meghan Hallam and Sam Bruno for field assistance; property owners on Samish Island for access to beach and quarry outcrops; Jim Hein and Tracey Conrad at the USGS for help with photomicrographs; and John Dewey for his review. Special thanks to Timothy Debacker whose critical review greatly improved the quality of the manuscript. Funding was provided by a Geological Society of America Student Research Grant, Western Washington University Research and Sponsored Programs, Western Washington University Geology Department, and University of Washington Earth and Space Sciences.

## Appendix. Supplementary material

Supplementary data associated with this article can be found in the online version, at doi:10.1016/j.jsg.2011.08.010.

## References

Anderson, M.W., Morris, A., 2004. The puzzle of axis-normal magnetic lineations in folded low-grade sediments (Bude Formation, SW England). In: Martín-Hernández, F., Lüneburg, C.M., Aubourg, C., Jackson, M. (Eds.), Magnetic Fabric: Methods and Applications. Geological Society of London Special Publication, vol. 238, pp. 175–190.

Anderson, T.B., 1964. Kink-bands and related geological structures. Nature 202, 272–274.

Anderson, T.B., 1974. The relationship between kink bands and shear fractures in the experimental deformation of slate. Journal of the Geological Society London 130, 367–382.

Brown, E.H., 1986. Geology of the Shuksan Suite. North Cascades, Washington, U.S.A. In: Geological Society of America Memoir, vol. 164, pp. 143–154.

Clifford, P., 1968. Kink-band development in the Lake St. Joseph area, northern Ontario. In: Baer, A.J., Norris, D.K. (Eds.), Research in Tectonics, vol. 68–52. Geological Survey of Canada paper, pp. 229–241.

Debacker, T.N., Seghedi, A., Belmans, M., Sintubin, M., 2008. Contractional kink bands formed by stress deflection along pre-existing anisotropies? Examples from the Anglo-Brabant deformation Belt (Belgium) and the North Dobrogea Orogen (Romania). Journal of Structural Geology 30, 1047–1059.

Dewey, J.F., 1965. Nature and origin of kink bands. Tectonophysics 1 (6), 459–494.

Dunham, R. E., 2010. Kink band development in the Darrington Phyllite on Samish Island, northwest Washington. M.S. thesis, Western Washington University.

Fyson, W.K., 1968. Profile variation in a kink set. In: Baer, A.J., Norris, D.K. (Eds.), Research in Tectonics, vol. 68–52. Geological Survey of Canada paper, pp. 243–254.
Gallagher, M.P., Brown, E.H., Walker, N.W., 1988. A new structural and tectonic interpretation of the western part of the Shuksan blueschist terrane, northwestern Washington. Geological Society of America Bulletin 100, 1415–1422.
Gay, N.C., Weiss, L.E., 1974. The relationship between principal stress directions and the geometry of kinks in foliated rocks. Tectonophysics 21, 287–300.
Haugerud, R. A., 1980. The Shuksan Metamorphic Suite and Shuksan Thrust, Mt. Watson area, North Cascades, Washington. M. S. thesis, Western Washington University.
Haugerud, R.A., Morrison, M.L., Brown, E.H., 1981. Structural and metamorphic history of the Shuksan metamorphic Suite in the Mount Watson and Gee point areas, North Cascades, Washington. Geological Society of America Bulletin 92, 374–383.
Hobson, D.M., 1973. The origin of kink bands near Tintagel, North Cornwall. Geological Magazine 100 (2), 133–144.
Housen, B.A., van der Pluijm, B.A., 1991. Slaty cleavage development and magnetic anisotropy fabrics. Journal of Geophysical Research 96, 9937–9946.
Hrouda, F., 1978. The magnetic fabric in some folds. Physics of the Earth and Planetary Interiors 17, 89–97.
Jones, M.A., 1999. Geologic Framework for the Puget Sound Aquifer System, Washington and British Columbia U.S. Geological Survey Professional Paper 1424-C.
Kirker, A.I., McClelland, E., 1997. Deflection of magnetic remanence during progressive cleavage development in the Pembrokeshire Old Red Sandstone. Geophysical Journal International 130, 240–250.
Kirschner, D.L., Teixell, A., 1996. Three-dimensional geometry of kink bands in slates and its relationship with finite strain. Tectonophysics 262, 195–211.
Lamb, R. M., 2000. Structural and tectonic history of the eastern San Juan Islands, Washington. M. S. thesis, Western Washington University.
Martín-Hernández, F., Kunze, K., Julivert, M., Hirt, A.M., 2005. Mathematical simulations of anisotropy of magnetic susceptibility on composite fabrics. Journal of Geophysical Research 110, B06102. doi:10.1029/2004JB003505.
Misch, P., 1966. Tectonic Evolution of the Northern Cascades of Washington State; A west-Cordilleran Case History, vol. 8. Canadian Institute of Mining and Metallurgy, Special volume, pp. 101–148.
Parés, J.M., van der Pluijm, B.A., 2002. Evaluating magnetic lineations (AMS) in deformed rocks. Tectonophysics 350, 283–298.
Paterson, M.S., Weiss, L.E., 1966. Experimental deformation and folding in phyllite. Geological Society of America Bulletin 77, 343–374.
Ramsay, J.G., 1967. Folding and Fracturing of Rocks. McGraw-Hill, New York.
Rousell, D.H., 1980. Kink bands in the Onaping formation, Sudbury Basin, Ontario. Tectonophysics 66, 83–97.
Schermer, E.R., Gillaspy, J.R., Lamb, R., 2007. Arc-parallel extension and fluid flow in an ancient accretionary wedge: the San Juan Islands, Washington. Geological Society of America Bulletin 119, 753–767.
Stewart, K.G., Alvarez, W., 1991. Mobile-hinge kinking in layered rocks and models. Journal of Structural Geology 13 (3), 243–259.
Tarling, D.H., Hrouda, F., 1993. The Magnetic Anisotropy of Rocks. Chapman & Hall, London.
Tauxe, L., 1998. Paleomagnetic Principles and Practice. Kluwer Academic Publishers, Dordrecht.
Twiss, R.J., Moores, E.M., 1992. Structural Geology. W. H. Freeman and Company, New York.
Verbeek, E.R., 1978. Kink bands in the Somport slates, west-central Pyrenees, France and Spain. Geological Society of America Bulletin 89, 814–824.
Weiss, L.E., 1980. Nucleation and growth of kink bands. Tectonophysics 65, 1–38.